16

A General Method of Terminal Truncation, Evolution, and Re-Elongation to Generate Enzymes of Enhanced Stability

Jochen Hecky, Jody M. Mason, Katja M. Arndt, and Kristian M. Müller

Summary

Improving enzyme stability is a highly desirable design step in generating enzymes able to function under extreme conditions, such as elevated temperatures, while having the additional benefit of being less susceptible to cleavage by proteases. For these reasons, many different approaches and techniques have been devised in constructing such proteins, but the results to date have been of mixed success. Here, we present a robust method involving the terminal truncation, random mutagenesis and fragmentation, recombination, elongation, and finally, selection at physiological temperatures, to generate an enzyme with improved stability. Three cycles of directed evolution comprising of random mutagenesis, DNA shuffling, and selection at 37°C were used, using the bacterial enzyme TEM-1 β-lactamase as a model protein to yield deletion mutants with in vivo ampicillin resistance levels comparable to wild-type (wt) enzyme. Kinetic studies demonstrate the selected mutant to have a significantly improved thermostability relative to its wt counterpart. Elongation of this mutant to the full-length gene resulted in a β-lactamase variant with dramatically increased thermostability. This technique was so fruitful that the evolved enzyme retained its maximum catalytic activity even 20°C above its wt parent protein optimum. Thus, structural perturbation by terminal truncation and subsequent compensation by directed evolution at physiological temperatures is a fast, efficient, and highly effective way to improve the thermostability of proteins without the need for selecting at elevated temperatures.

Key Words: Protein stabilization; protein stability; terminal truncation; thermostability; enzyme activity; DNA shuffling; random mutagenesis; elongation.

1. Introduction

If an enzyme were able to be modified for increased stability, a number of new options could become open for exploitation. For example, the protein would be active over a greater range of temperatures, and would be likely to have an

From: *Methods in Molecular Biology, vol. 352: Protein Engineering Protocols*
Edited by: K. M. Arndt and K. M. Müller © Humana Press Inc., Totowa, NJ

improved half-life resulting from a lower sensitivity to proteases. Stability, together with increased specificity and activity, is one of the most sought-after properties of a protein to be improved and applied either industrially or pharmacologically.

A large number of factors enhancing thermostability has been identified so far *(1–4)*. Examples include increased rigidity and compactness, more core hydrophobic residues, and increased van der Waals interactions. Improved thermostability can also be achieved by the introduction of metal binding sites, additional disulfide bridges *(5,6)*, backbone cyclization, and by the shortening or deletion of loop regions *(7)*. Two of the main factors of high protein thermostability seem to be increased hydrogen bonding and the formation of ionic interaction networks *(8–10)*.

However, because a complete understanding of thermostability at the molecular level remains elusive *(11)*, the generation of thermostable proteins continues to be a challenging task. Computational and comparative approaches have been established to aid in the identification of stabilizing interactions and both have been applied successfully for these purposes *(12–14)*. However, they rely either on the presence of a well-resolved crystal or nuclear magnetic resonance structure, that is, a defined Cα trace, or on the availability of numerous homologous sequences, preferably from thermophilic sources. In addition, evolutionary approaches mimicking the Darwinian optimization cycle "mutagenesis, recombination, and selection" have been introduced to overcome the boundaries of current rational protein design *(15,16)*.

1.1. Terminal Truncations

The importance of the terminal regions of proteins for structural or functional integrity varies from protein to protein. Some proteins readily tolerate the removal of terminal residues without any impairment of the native three-dimensional structure and conformational stability, which is in line with the observation that, in crystal structures, the terminal sections are frequently either poorly defined or not ordered at all. In contrast, some proteins are very sensitive to terminal shortening. In this case, the removal of several terminal residues can result in a large reduction in conformational stability, a looser structure *(17)*, and an enhanced susceptibility to proteolysis or aggregation *(18)*. This has been demonstrated for RNase A *(19)*, RNase HI *(20)*, Staphylococcal nuclease R *(17)*, Rhodanese *(21,22)*, the Stoffel fragment of *Taq* DNA polymerase *(23)*, and chloramphenicol acetyl transferase *(18)*. Although some proteins may not tolerate the removal of even a single terminal amino acid residue, for the majority of proteins, a threshold level of truncation seems to exist within which the expression level, the native conformation, and the stability are significantly affected although they are still compatible with protein function under certain circumstances (e.g., lowered reaction temperature).

Beyond this threshold, however, truncations lead to irreversible damaging of the protein structure and result in a complete loss of function. Therefore, by carefully selecting the correct degree of truncation, structural perturbations can be introduced easily in many protein structures without interfering with the folding process and a functional conformation.

1.2. Compensation of Structural Perturbations by Directed Evolution

Structural perturbations introduced into a protein by amino acid exchanges, insertions, or deletions can be reversed by single or multiple compensatory mutations, which often act as so-called global or second-site suppressors ***(24)*** because they suppress the phenotypes of various otherwise detrimental mutations at sites distant to the primary exchanges. This phenomenon follows from the high complexity and plasticity of protein structures and the intramolecular interaction networks governing protein stability. In the end, it is facilitated by the degenerate nature of protein structures, which are determined essentially by a limited number of key residues, whereas a large number of residues can be replaced without any phenotypic effect. Second-site suppressors of truncated versions of RNase HI have been created and identified by random mutagenesis followed by selection of functional variants ***(20)***. However, the introduction of mutations by a random mutagenic process alone is likely to be accompanied by the accumulation of detrimental mutations reducing the number of functional proteins and, thus, the number of testable beneficial mutations. To overcome the limitations of random mutagenesis alone, a combinatorial process known as DNA shuffling has been introduced ***(15,16)***, marking a cornerstone in the field of DNA-based protein manipulation. The resulting approach comprises repeated cycles of creation and jumbling of point mutations, and is referred to as in vitro or directed evolution. It is based on the same principles that govern natural evolution, namely, random mutagenesis, recombination, and screening or selection. Using this approach, many enzymes have since been improved considerably in terms of activity, selectivity, stability, and even function in organic solvents ***(25)***. Directed evolution features many advantages over rational approaches because no previous knowledge of three-dimensional structure is required to improve enzyme properties. However, its applicability is strictly restricted to those proteins for which appropriate screening or, even better, selection procedures exist.

This chapter summarizes a manageable, widely applicable approach for the improvement of the stability of proteins. It is based on the introduction of structural perturbations by trimming the chain ends of a target protein at the DNA level (**Subheadings 3.2.** and **3.3.**). The detrimental phenotypes accompanying the truncations (**Subheading 3.4.**) are overcome by an evolutionary, genetic in vitro optimization procedure (**Subheading 3.5.**). The resulting truncation–optimization –elongation approach (**Fig. 1A**) stands out from other techniques by its simplicity because it relies neither on available structural

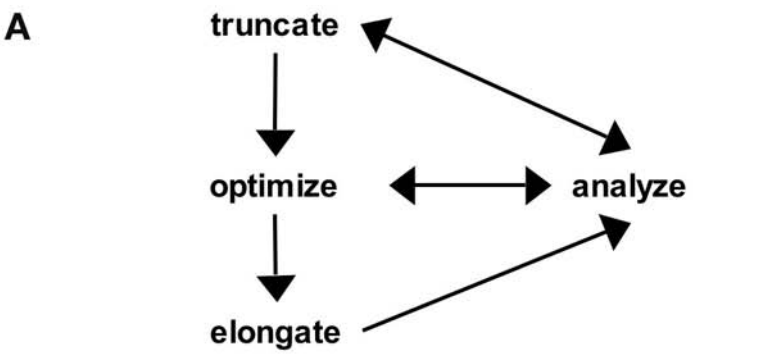

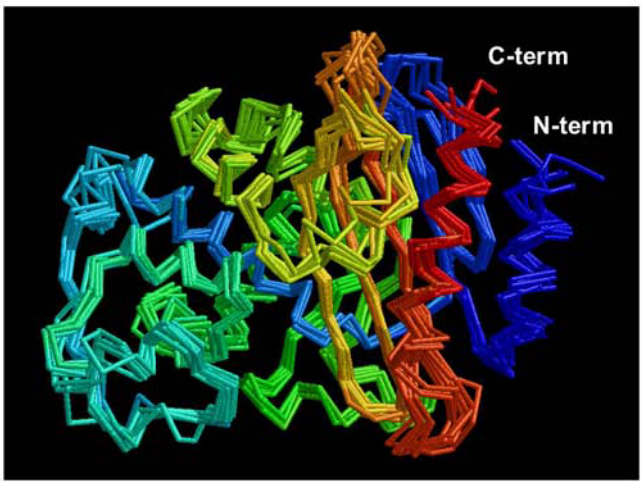

C

```
1BTL/        HPETLVKVKDAEDQL ~ MDERNRQIAEIGASLIKHW
1TEM
1SHV:A       spQPLEQIKLSESQL ~ MAERNQQIAGIGAALIEHWqr
1MBL:B       ktemkDDFAKLEEQF ~ ---
DDKLIAEATKVVMKalnmng
1BZA         anSVQQQLEALEKSS ~ R--RRDILAAAAKIVThgf
1BUL         ntkGIDEIKNLETDF ~ H--EDKVIAEASRIAIdnlk
1BSG   ghgsgsvsDAERRLAGLERAS ~ R--DDGLVADAARVLAETLg
1MFO         -APIDDQLAELERRD ~ N--LRPLIGELTALVLPSLl
1PIO:A       ----mKELNDLEKKY ~ P--NDKLISETAKSVMKEF--
```

Fig. 1. **(A)** Scheme of truncation–optimization–elongation. The enzyme is truncated, optimized by directed evolution, and, finally, elongated to the full-length protein. All steps

information nor on the existence of known homologous proteins. However, if this kind of information can be obtained using the multitude of current databases, the truncation design process will be, of course, more straightforward, and, in some cases, more efficient. Finally, the described approach features an additional benefit because it allows the generation of thermostable enzyme variants with the selection being performed at physiological temperatures.

2. Materials

2.1. Plasmid Construction, DNA Shuffling, and Random Mutagenesis

1. Forward primer pr_sfi_pelB_DG_blawt: 5′-TTACTCACGGCCCAGCCGGCCATGGCTGACGG **TCACCCAGAAACGCTGGTG**-3′; restriction sites are underlined and hybridizing regions are in bold.
2. Forward primer pr_sfi_pelB_DG_bladelHPE: 5′-TTACTCGCGGCCCAGCCGGCCATGGCTGACGGT**ACGCTGGTGAAAGTAAAAGATG**-3′.
3. Forward primer pr_sfi_pelB_DG_bladelHPETL: 5′-TTACTCACGGCCCAGCCGGCCATGGCTGACGGT**GTGAAAGTAAAAGATGCTGAAG** -3′.
4. Reverse primer pr_blawt_GG_his5_hind: 5′-TAGTCAAGCTTACTAGTGATGGTGATGGTGGCCACC**CCAATGCTTAATCAGTGAGG**-3′.
5. Reverse primer pr_bladelW_GG_his5_hind: 5′-TAGTCAAGCTTACTAGTGATGGTGATGGTGGCCACC**ATGCTTAATCAGTGAGGCACC**-3′.
6. Reverse primer pr_bla_delKHW_GG_his5_hind: 5′-TAGATCAAGCTTACTAGTGATGGTGATGGTGGCCACC**AAT CAGTGAGGCACCTATCTC**-3′.
7. Plasmid pKMENGRbla, a derivative of pAK400 ***(26)***.
8. Restriction enzymes *Sfi*I and *Hin*dIII (NEB).
9. Plasmid pKJE_Bla-NΔ5: expresses the TEM-1 β-lactamase with the first five N-terminal residues deleted (*see* **Subheading 3.3.**).
10. Forward primer pr_sfi_pelB_DG_shuffl: 5′-TTACTCACGGCCCAGCCGGCCATGGCTGACGG-3′; restriction sites are underlined.

Fig. 1. *(Continued)* can be analyzed for activity and stability. **(B)** Superimposed Cα traces show various β-lactamases from different bacterial species using the CE algorithm ***(30)***. Contiguous secondary structural elements are in different shades of gray, using RasMol ***(47)***. **(C)** Structure-based sequence alignment of the N- and C-terminal parts of the β-lactamases displayed in (B), corresponding to the N- and C-terminal helix of the TEM-1 enzyme (PDB entries 1btl/1tem) are shown. Sequences are specified by given PDB codes. Residues that were ignored by the CE algorithm and are, therefore, not included in the superposition, are given in lowercase letters. Residues present in the SWISSPROT database, but missing in the corresponding X-ray structure, are indicated in italics. Omitted parts of the sequence are symbolized by ~. Selected β-lactamase genes showed identity ranging from 67.8 to 32.4%. Corresponding structures had root mean square deviation values ranging from 1.2 to 2.2 Å (with reference to the TEM-1 β-lactamase) and Z-scores greater than 7. The structural superposition demonstrates the structural variability of the terminal helices.

11. Reverse primer pr_GG_his5_hind_shuffl: 5′-TAGTCAAGCTTACTAGTGATG-GTGATGGTGGCCACC-3′.
12. *Taq* DNA polymerase (Sigma).
13. DNase I (Sigma).
14. DNase buffer: 50 m*M* Tris-HCl, pH 7.5, and 1 m*M* $MgCl_2$.
15. EDTA solution: 0.5 *M* EDTA.
16. Agarose gel: 1 to 2% (w/v) agarose in 0.5X Tris-base–boric acid–EDTA (TBE) buffer.
17. 10X TBE buffer: 1 *M* Tris-base, 1 *M* boric acid, and 20 m*M* EDTA, pH 8.0.
18. QiaexII gel extraction kit (Qiagen).
19. dNTP (Amersham).
20. Thermocycler (Eppendorf).
21. $MgCl_2$ stock solution: 25 to 100 m*M* $MgCl_2$.
22. $MnCl_2$ stock solution: 5 m*M* $MnCl_2$.
23. GFX polymerase chain reaction (PCR) DNA and gel band purification kit (Amersham).

2.2. Transformation, Protein Expression, and Purification

1. Butanol.
2. Electrocompetent *Escherichia coli* XL-1 Blue cells.
3. Electroporator (Bio-Rad).
4. 2YT: dissolve 16 g bacto-tryptone, 10 g yeast extract, and 5 g NaCl in 1 L H_2O and autoclave.
5. Transformation salt stock: 250 m*M* KCl and 1 *M* $MgCl_2$.
6. Ampicillin stock solution: dissolve 100 mg/mL ampicillin in water and filter through 0.22-µm, aliquot, and store at –20°C.
7. LB/Cm agar plates: 1% bacto-tryptone, 0.5% yeast extract, 0.5% NaCl, 1.5% agar, and 25 µg/mL chloramphenicol.
8. LB/Cm: 1% bacto-tryptone, 0.5% yeast extract, 0.5% NaCl, 1.5% agar, and 25 µg/mL chloramphenicol.
9. 2YT/Cm: 2YT medium supplemented with 25 µg/mL chloramphenicol.
10. High-speed centrifuge (Sorvall, with GS-3 and SS-34 rotor).
11. Resuspension buffer: 50 m*M* sodium phosphate and 500 m*M* NaCl, pH 7.0.
12. Benzonase (Sigma).
13. 0.45-µm polyethersulfone syringe filter.
14. 2-mL phenylboronate columns (MoBiTec).
15. Borate buffer: 0.5 *M* borate and 0.5 *M* NaCl, pH 7.0.
16. 4-mL Ni-nitrilotriacetic acid (NTA) column: 4 mL Ni-NTA superflow matrix (Qiagen) in a C10/10 column (Amersham-Pharmacia).
17. Imidazole buffer: 50 m*M* sodium phosphate, 0.25 *M* imidazol, and 50 m*M* NaCl, pH 7.0.
18. Phosphate buffer: 50 m*M* sodium phosphate and 150 m*M* NaCl, pH 7.2.
19. EDTA.
20. 1-mL phenylsuperose HR 5/5 column (Amersham-Pharmacia).

21. Tris-HCl buffer: 25 m*M* Tris-HCl and 25 m*M* NaCl, pH 8.0.
22. Mono Q HR 5/5 column (Amersham-Pharmacia).
23. Tris-HCl–NaCl buffer: 25 m*M* Tris-HCl and 0.5 *M* NaCl, pH 8.0.

2.3. Enzyme Assays and Urea-Induced Unfolding

1. Nitrocefin solution: 0.2 m*M* nitrocefin, 50 m*M* potassium phosphate and 0.5% dimethylsulfoxide, pH 7.0.
2. Photospectrometer that can at least measure one data point per second, e.g., Ultrospec 3000 (Amersham-Pharmacia) or V-550 (Jasco).
3. Spectrofluorometer, e.g., FluoroMax-2 (Jobin-Yvon) or FP-6500 (Jasco).
4. Phosphate buffer (*see* **Subheading 2.2., item 18**).
5. Urea: ultrapure, at least 99% purity (ICN).

3. Methods

This chapter presents a general method to increase the thermostability of proteins without the need of screening for activity at elevated temperatures. After an introduction of our model system, β-lactamase (**Subheading 3.1.**), we describe the design considerations for terminal truncations (**Subheadings 3.2.** and **3.3.**) and their effect on enzyme activity (**Subheading 3.4.**). Libraries are generated by directed evolution and error-prone PCR (**Subheading 3.5.**), and selected in vivo by applying different selection stringencies (**Subheading 3.6.**). The last part of this chapter discusses the re-elongation of evolved truncation mutants (**Subheading 3.7.**), expression strategies and purification methods (**Subheading 3.8.**), and enzymatic assays (**Subheading 3.9.**) and stability tests (**Subheading 3.10.**) for characterization.

3.1. β-Lactamase as a Model System

To demonstrate the applicability of the truncation–optimization–elongation approach (**Fig. 1A**) for the improvement of thermostability, TEM-1 β-lactamase was chosen as a model system. As a clinically relevant pathogenesis factor and important resistance marker, it belongs to a well-characterized family of proteins, for which several crystal structures are available. In addition, many mutagenic studies have been performed facilitating the study and interpretation of structure–function relationships and the rational design of truncations. Furthermore, β-lactamase is used for prodrug activation cancer therapy, making a stable β-lactamase a potential lead compound ***(27,28)***.

Class A β-lactamases (EC 3.5.2.6) are bacterial periplasmic enzymes with relatively diverse amino acid sequences and stabilities but very similar tertiary structures. Although the polypeptide backbones of class A β-lactamases superimpose particularly well in the core region, they do so poorly at the ends of the terminal helices. The structural differences at the termini are accompanied by a

high variability in length and amino acid composition of these regions, making these enzymes well-suited to test general ideas regarding the relation of sequence homology and functional importance.

3.2. Design of Terminal Truncations

The correct design of the deletions constitutes a central step in the approach described here: if the termini are shortened by too many residues, the resulting truncation variant is likely to be nonfunctional because of insufficient stability or defective folding; alternatively, if not enough residues are removed, it is unlikely that an impaired phenotype will arise and, thus, no selection pressure can be imposed on the gain of stabilizing exchanges.

If a crystal structure of the protein of interest exists, the Protein Data Bank (PDB; http://www.pdb.org/), SWISSPROT (http://www.expasy.org/sprot/ and http://www.ebi.ac.uk/swissprot/), and SCOP (http://scop.mrc-lmb.cam.ac.uk/scop/) databases in combination with structure analysis tools, such as the molecular modeling program WHATIF (http://swift.cmbi.kun.nl/WIWWWI/) and the CE algorithm (http://cl.sdsc.edu/ce.html) can be used for structural comparison and analysis. In particular, contact maps can be used to identify possible nonessential and essential interactions, which may help in the design process. If no high-resolution structure is available, other databases (e.g., HSSP) and the SWISS-MODEL homology-modeling server (http://swissmodel.expasy.org) can be applied, or, alternatively, sequential deletions in one or two amino acid steps can be performed to define the threshold level.

In this study, four different truncation variants were planned using information from mutagenic studies *(29)*, a structure-based alignment of various homologous class A β-lactamases, and structural analysis using the CE algorithm *(30)* and the SWISS-PDB Viewer (http://www.expasy.org/spdbv) *(31)*, respectively (**Fig. 1B,C**). The truncations were intended to introduce structural perturbations at physiological temperatures without rendering the protein completely nonfunctional. The first three residues at the N-terminus (His, Pro, and Glu) have high temperature factors (up to 23.8 $Å^2$; average: 13.1 $Å^2$) and solvent accessibilities (PDB code 1btl), and their deletion (yielding the mutant NΔ3) was expected to affect stability only marginally. The second N-terminal truncation (NΔ5) included the adjacent threonine and leucine, the first of which is nearly completely buried and forms a hydrogen bond to Ser285 of the C-terminal helix. At the C-terminal end, only one or three residues (mutants CΔ1 and CΔ3) were removed, because the distal tryptophan has been shown to be "essential" in a previous study *(32)*.

3.3. Plasmid Design

The plasmids were designed to encode the mature wild-type (wt) β-lactamase or the respective deletion mutants as fusion proteins with an N-terminal pelB

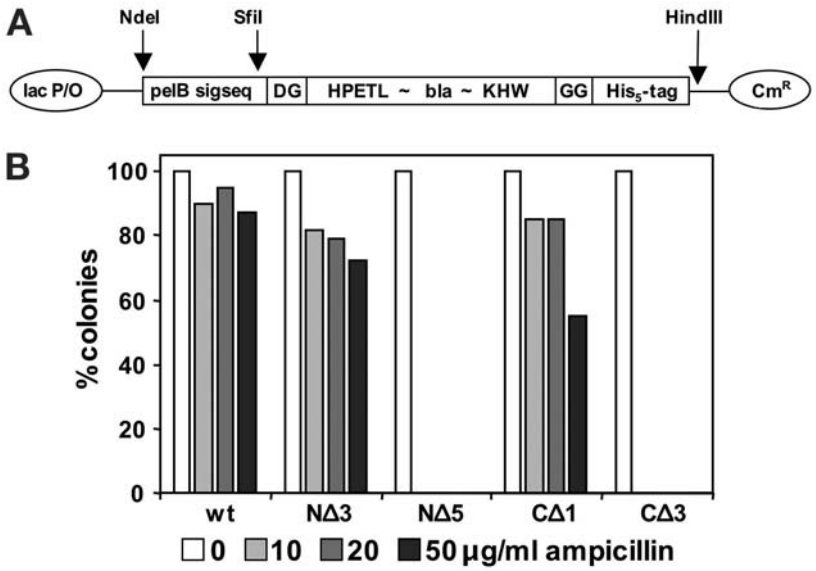

Fig. 2. **(A)** Expression vector design. A pelB signal sequence followed by aspartate and glycine was fused to the coding region of mature TEM β-lactamase, which was followed by two glycine residues and a His_5-tag to facilitate purification. Important endonuclease restriction sites are shown. For cytoplasmically expressed variants, the pelB signal sequences and aspartate/glycine residues were replaced by a single methionine residue. All plasmids contained a chloramphenicol resistance gene. **(B)** In vivo fitness of initially generated β-lactamase deletion mutants. Approximately 3500 freshly transformed XL-1 Blue cells harboring the respective plasmid were selected on LB agar plates containing chloramphenicol and 10 to 50 µg/mL ampicillin or chloramphenicol alone (100% clones). Plates were analyzed after 20 h incubation at 37°C. For the NΔ5-clone and CΔ3-clone, no colonies could be observed in the presence of ampicillin.

signal sequence ***(33)*** required for periplasmic targeting. A short aspartate–glycine linker was included to ensure an equally efficient processing rate for the variants that differ in their N-termini. Finally, a C-terminal His-tag was inserted to allow for immobilized metal ion affinity chromatography (IMAC), even of nonnative β-lactamase variants (**Fig. 2A**).

The plasmids were constructed as follows:

1. TEM-1 β-Lactamase deletion mutants, named NΔ3-clone, NΔ5-clone, CΔ1-clone, and CΔ3-clone, were generated by amplifying the *TEM*-1 gene from a pUC-derived plasmid ***(34)***, using the respective forward and reverse primers. The forward primers provided the resulting PCR products with a 5′ *Sfi*I restriction site for cloning, the coding sequence for the C-terminal part of a pelB signal peptide, an aspartate–glycine linker, and the respective N-terminal modification (truncation) of the TEM-1 variants. At the 3′-end of the gene, the reverse primers introduced the

coding sequence for the modified TEM-1 C termini, a short spacer (two glycine residues), and a penta-histidine tag, two stop codons, and a *Hin*dIII restriction site.
2. The PCR products were digested with *Sfi*I/*Hin*dIII, isolated, and cloned into the *Sfi*I/*Hin*dIII fragment of pKMENGRbla (provided by K. M. M., unpublished), a derivative of the expression plasmid pAK400 ***(26)***, which carries a chloramphenicol resistance gene.

The resulting plasmids (pKJE_Bla-NΔ/CΔ series) expressed the various *TEM*-1 genes under control of a *lac* promoter/operator region. Despite the constitutive expression of *lac*I on the plasmids, a strong phage T7g10 Shine-Dalgarno sequence ***(35)*** resulted in a relatively high basal gene expression level. Therefore, all selection steps were performed under stringent conditions without overexpression.

3.4. Effect of Terminal Truncation on Enzyme Activity

The effect of the terminal truncations on enzyme activity can be estimated using growth assays on petri dishes or in liquid cultures in the presence of increasing concentrations of ampicillin. In general, selection on plates is more stringent than in liquid culture. Stringency can additionally be varied by looking at basal gene expression or after induction with isopropylthiogalactoside (IPTG), and also by incubating at different temperatures.

1. If necessary, transform the plasmids in BL21 cells using standard methods and plate on LB/Cm agar plates.
2. Grow overnight cultures started from glycerol stocks or from single colonies on plates (**step 1**) in LB/Cm for approx 16 h.
3. From the overnight culture, inoculate a preculture at an optical density (OD) at 600 nm (OD_{600}) of 0.1 and grow the culture to an OD_{600} of 1 (*see* **Note 1**).
4. Plate an aliquot of the preculture from **step 3** on LB/Cm agar plates with various amounts of ampicillin with or without IPTG. The amount needed for plating can be estimated by approximating that 2.5×10^8 cells/mL have an OD_{600} of 1.
5. Alternatively, inoculate a liquid LB/Cm culture with the preculture from **step 3** (starting $OD_{600} = 0.1$) with various amounts of ampicillin with or without IPTG.
6. Growth assays (**steps 4** and **5**) can be repeated at various incubation temperatures.

Without induction, colony numbers of cells producing any of the deletion mutants decreased significantly if the selective pressure increased from 0 to 50 µg/mL ampicillin on plates incubated at 37°C (**Fig. 2B**). For the mutants, NΔ5-clone and CΔ3-clone, no colonies were observed after 40 h incubation, suggesting an important role for the terminal residues. With induction, cells harboring the NΔ5-clone grew on plates with up to 50 µg/mL ampicillin at 25°C and in liquid culture with optimal aeration also at 37°C. This suggests that both truncations induced structural perturbations, but, at the same time, allowed for folding into active states. The NΔ5-clone conferred resistance to a much lower extent than the CΔ3-clone and was, therefore, chosen for subsequent optimization.

3.5. DNA Shuffling and Random Mutagenesis

The central step of every optimization procedure designed to reverse the structural perturbations brought about by terminal shortening or the introduction of deleterious mutations is the generation of a highly diverse library of variants at the genetic level. Random mutagenesis alone as well as in combination with DNA recombination has been harnessed to raise the required mutations.

DNA shuffling ***(15,16)*** is a widely used method for DNA recombination in the test tube. Because the jumbling of different homologous DNA sequences realized by DNA shuffling marks a crucial step of directed evolution, its central aspects should be depicted here in short: after the random generation of point mutations along the entire gene, primarily by error-prone PCR (*see* **step 7**) the resulting library of genes is subjected to DNA fragmentation to produce short, slightly different, interchangeable sequences of approx 50 to 200 basepairs length. Overlapping homologous sequences differing in one or more nucleotides are then assembled into larger fragments by a PCR procedure, starting with low annealing temperatures to allow mutual priming of the smallest fragments present in the mixture. With increasing cycle numbers, the annealing temperature is elevated steadily to select for longer overlaps favoring larger fragment sizes. Finally, the complete gene is fully assembled and amplified using a pair of flanking primers that overlap the terminal nucleotides of the gene and provide the resulting library with appropriate restriction sites for subsequent cloning.

The following section includes concrete instructions for how random mutagenesis and DNA shuffling can be performed to create a library of sufficient complexity to find some needles in a large haystack of sequence space. Note that the procedure described here is optimized with respect to our test system and might have to be modulated depending on the composition and length of the target gene. It should be taken into account that the usual order of reactions—first random mutagenesis, second recombination—was not kept here to determine the error rate of the shuffling process itself before the generation of point mutations by error-prone PCR (*see* **Note 2**).

1. Produce sufficient amounts (5–10 µg) of the gene of interest, either by PCR using primers homologous to constant regions flanking the target gene, or by the use of restriction enzymes cutting near to the ends of the gene. If PCR is used, *Taq* DNA polymerase should be used throughout to augment misincorporation of nucleotides. In our example, we amplified the truncated β-lactamase using the plasmid pKJE_BlaNΔ5, and the primers pr_sfi_pelB_DG_shuffl and pr_GG_his5_hind_shuffl.
2. Digest approx 4 to 5 µg of the target gene using 0.2 U DNase I in a total volume of 50 µL DNase buffer for 12 min at room temperature (25°C).
3. Stop the endonucleolytic degradation process by adding 4 µL EDTA solution and storing on ice.

4. Analyze the resulting DNA fragments on a 2% (w/v) agarose gel and excise fragments of approx 50 to 150 basepairs length.
5. Purify the fragments using the QiaexII gel extraction kit (*see* **Note 3**).
6. Assemble approx 100 to 300 ng of the isolated fragments in a primer extension PCR in a total volume of 50 µL (*see* **Note 4**). The reaction mix contains 2.5 U *Taq* DNA polymerase, 0.4 m*M* of each dNTP, and 2 m*M* $MgCl_2$ in the supplied *Taq* buffer. Assembly PCR reactions are carried out, for example, in a thermocycler (Eppendorf) using the following program: 94°C for 3 min; 10 cycles of: 94°C for 1 min (denaturation), 45°C + 0.3°C/cycle for 1 min (annealing), 72°C for 1 min (elongation), and 72°C for 5 min after the last cycle; 15 cycles of: 94°C for 1 min, 50°C + 0.4°C/cycle for 1 min, 72°C for 1 min, 72°C for 5 min after the 15 cycles; 10 cycles of: 94°C for 1 min, 56°C + 0.5°C/cycle for 1 min, 72°C for 1 min, and 72°C for 5 min after the last cycle; 10 cycles of: 94°C for 1 min, 61°C + 0.5°C/cycle for 2 min, 72°C for 2 min, and 72°C for 5 min after the 10 cycles. Alternatively, a simplified program can be used consisting of: 94°C for 3 min; 35 cycles of: 92°C for 30 s, 30°C + 1°C/cycle for 1 min, 72°C for 1 min + 4 s/cycle, and 72°C for 5 min after the final cycle.
7. Amplify 1/5 volume of the assembly PCR reaction (no purification required) to ensure full length of the reconstituted genes and to add the appropriate restriction sites required for subsequent cloning. This step can be done at error-prone conditions to extend the library diversity. In addition to using *Taq* DNA polymerase for elongation, the error-rate of the amplification reaction can be increased by including 7 m*M* $MgCl_2$ and 0.5 m*M* $MnCl_2$ in the reaction mixture ***(36)*** (*see* **Note 5**). In our example, we used primers pr_sfi_pelB_DG_shuffl and pr_GG_his5_hind_shuffl at a final concentration of 0.5 µ*M* each. The reaction mixture included 7 m*M* $MgCl_2$, 0.5 m*M* $MnCl_2$, each dNTP at 0.4 m*M*, and 2.5 U *Taq*. The program used was 3 min at 94°C, 25 cycles of 1 min at 94°C, 1 min at 68°C, and 1 min at 72°C, with a final step of 7 min at 72°C.
8. Purify the PCR products using, e.g., the GFX PCR DNA and Gel Band Purification Kit, digest it with the appropriate enzymes (*Sfi*I and *Hin*dIII) and clone it into the expression vector (pKJE_Bla-ΔN5) treated with the same enzymes. Transformation is performed as described in **Subheading 3.6.**

We performed three rounds of directed evolution (S1 to S3) using the DNA shuffling and random mutagenesis procedures in combination with in vivo selection steps. Clones selected were pooled and served as templates for subsequent rounds. In the last round of directed evolution, the error-prone PCR step after DNA shuffling was replaced by a standard PCR procedure to prevent the introduction of deleterious mutations into the recombined clones.

3.6. Transformation and In Vivo Selection of Mutant Libraries

1. Desalt the plasmid mutant libraries (pKJE_Bla-NΔ5_Lib-S1 to -S3; S indicates shuffling rounds one to three, *see* **Subheading 3.5.**) by butanol precipitation. To 10- to 20-µL ligation mixtures, add double-distilled water to a volume of 50 µL. Mix thoroughly with 500 µL butanol and spin at maximal speed (~2000*g*) at room

temperature for 30 min. Remove supernatant, air-dry, and dissolve the pellet in 10 to 20 µL of water.

2. Transform desalted DNA into 100 µL of electrocompetent *E. coli* XL-1 Blue cells using 1.7 kV, 200 Ω, and 25 µF. Immediately after transformation, add 900 µL 2YT and 1/100 volume of transformation salt stock.
3. Transfer the cell suspensions in 10-mL glass test tubes and incubate for 60 to 70 min at 37°C with orbital shaking.
4. Assess the transformation efficiency by plating a dilution series of each transformation mixture on LB/Cm agar.
5. Use another aliquot of the transformed cells to estimate the level of selection pressure for the following round by plating on LB/Cm agar plates supplemented with various concentrations of ampicillin (*see* **Note 6**). Take the highest ampicillin concentration at which colonies can be observed as selection level for the subsequent round.
6. For selection, plate the transformed cells on LB/Cm agar plates with the ampicillin concentration determined in **step 5** (*see also* **Note 6**). We used ampicillin concentrations of 20 µg/mL, 100 µg/mL, and 200 µg/mL for the first, second, and third selection, respectively. The first selection round was performed in liquid medium, the other two rounds were selected on agar plates.

The impaired truncation mutant NΔ5-clone was revitalized by three rounds of directed evolution comprising random mutagenesis and DNA shuffling of a PCR product (as described in **Subheading 3.5.**). In three successive rounds, approx 19×10^3, 147×10^3, and 260×10^3 clones were generated and screened for survival on plates containing 20, 100, and 200 µg/mL ampicillin (*see* **step 6**), respectively, giving rise to approx 3, 600, and 7000 colonies.

Table 1 summarizes all sequenced clones isolated in the course of directed evolution sorted by shuffling round (S1–S3). Additionally, **Table 1** includes relative solvent accessibilities and average side chain atomic temperature factors (taken from PDB 1btl) ***(37)*** for each of the substituted wt residues. The five clones sequenced after the second optimization round shared two mutations, M182T and T265M (numbering according to Ambler et al., **ref.** ***38***), which were already present after the first round.

After the final optimization step, the library was pooled, and the maximum level of ampicillin resistance was determined on plates without IPTG, as described in **Subheading 3.4.** (**Fig. 3**). Normal colony development of a significant number of clones was seen up to 700 µg/mL, and, after prolonged incubation times of 40 h, clones could even be detected on 1000 µg/mL. In contrast, the wt construct grew only up to 500 µg/mL. Twenty-six clones were picked from the 800 to 1000 µg/mL plates and sequenced. The 26 sequences corresponded to 15 individual clones (**Table 1**). All clones shared two mutations, M182T and A224V. The M182T mutation has previously been demonstrated to compensate for folding defects ***(39)*** and stability losses ***(29,40)***. The second mutation (A224V) prevailed at the increased selective pressure of the third round. This

Table 1
Amino Acid Substitutions Selected in the Course of Directed Evolution of the NΔ5 Deletion Mutant

position	31	37	38	42	52	56	59	63	82	84	88	96	104	120	147	150	153	159	168	177	182	192	195	198	206	208	224	240	247	256	265	277
wt	V	E	D	A	N	I	S	E	S	I	Q	H	E	R	E	A	H	V	E	E	M	K	T	L	Q	I	A	E	I	K	T	R
% acc	63.3	15.1	55.7	18	84.3	45.8	28.7	66.3	24	19.1	59.9	68.2	66.3	47.4	50.1	40.1	51.1	25.9	54.2	48.1	20.3	36	45.5	40.7	25.6	18.5	27.5	56.5	0	73.1	4.7	60.8
B factor (sc)	8.3	12.2	19.9	11.6	16.7	8.7	11.0	25.5	8.8	13.8	33.5	20.7	34.1	25.0	20.6	8.3	16.5	6.5	21.1	23.5	7.9	12.1	14.6	25.7	14.0	13.8	8.2	26.1	5.4	26.0	7.0	30.9
S1/1																			A		T										M	
S1/2													G								T		S				V			R		
S1/3																	R												V			
S2/1																	R				T				H		V				M	
S2/2															G					K	T										M	
S2/3																					T										M	
S2/4				G															A		T	E	S				V				M	
S2/5																					T										M	
S3/1 (×2)					S					V					G				V		T						V					
S3/2 (×4)														G			R	A			T						V					
S3/4 (×3)		D										Y									T						V				M	
S3/5 (×4)	A													G							T						V		V			
S3/6																	R				T		S				V					
S3/7 (×3)							G			V											T		F				V		V			
S3/17										V											T						V					
S3/18										V							R				T		S				V					
S3/19														G							T						V	G			M	K
S3/20	A		N	G					F	V											T		S	P			V		V	R	M	
S3/21	A																R				T		S				V					
S3/22									E		E						R		A		T						V			R		
S3/23					D			K		V						T	R				T		S	P			V					
S3/24						T				V							R				T					M	V					
S3/26																	R				T					M	V					
position	31	37	38	42	52	56	59	63	82	84	88	96	104	120	147	150	153	159	168	177	182	192	195	198	206	208	224	240	247	256	265	277

Amino acid substitutions of the selected deletion mutants are shown with regard to wt sequence. Residues are numbered according to Ambler et al. *(38)*. Mutants are grouped according to the round of directed evolution in which they were selected (S1–S3). The frequency of individual selected clones containing the same set of mutations is shown in brackets. The most prevalent amino acid substitutions of the third round mutants are shown in boldface type. % acc, relative solvent accessibility, the ratio between calculated and vacuum accessibility expressed as a percentage using the program What If *(48)*; B-factors corresponding to the average of side-chain atoms were taken from the Protein Data Bank (PDB entry: 1btl).

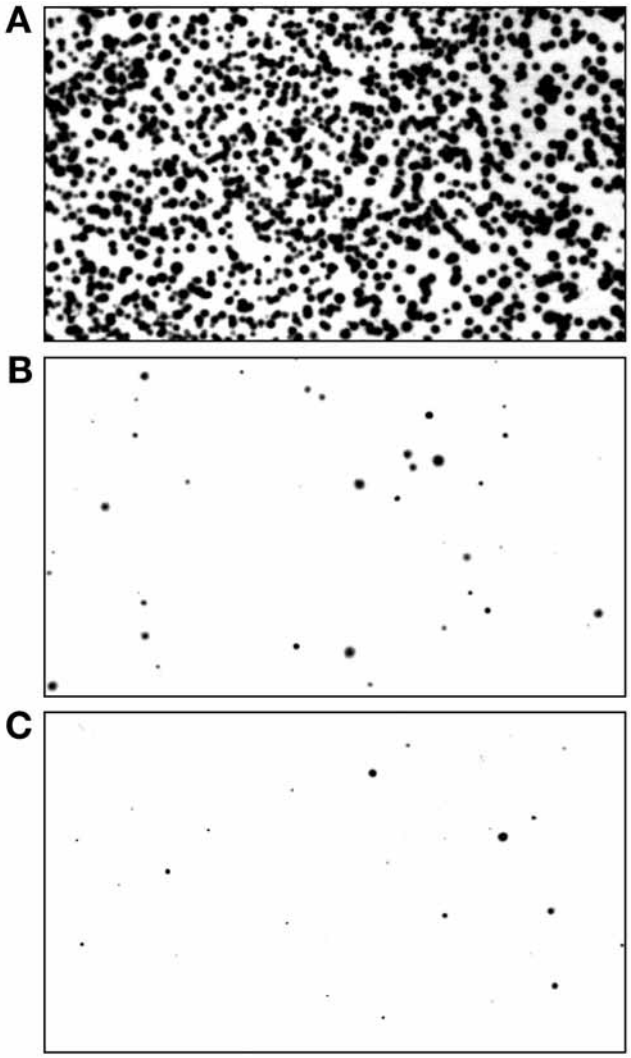

Fig. 3. Colonies of optimized NΔ5-β-lactamase deletion mutants on LB agar plates containing **(A)** no, **(B)** 350 μg/mL, or **(C)** 700 μg/mL ampicillin. Approximately 1500 cells of a regrown culture of pooled colonies isolated in the third round of directed evolution were plated. Plates are photographed after (A) 20 h or (B and C) 40 h incubation at 37°C.

mutation has been listed once, but no experiments were performed with this mutant ***(41)***.

Both mutations are at least 17 Å away from the site of deletion, indicating independent compensation of the structural interference imposed by deletion. **Figure 4** highlights the most-frequently mutated residues mapped to the known tertiary structure of TEM-1 β-lactamase. In general, the sets of mutations found

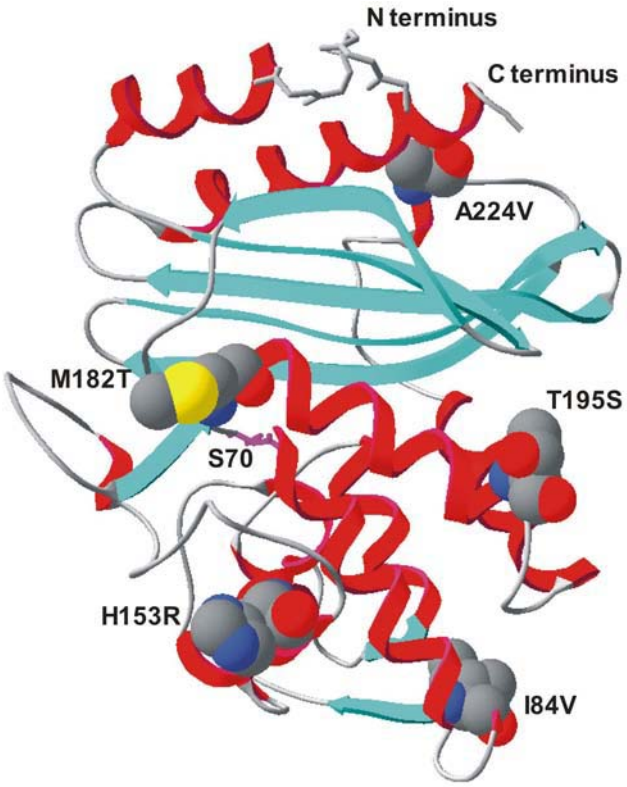

Fig. 4. Structure of wt TEM-1 β-lactamase (PDB identifier: 1btl). Residues frequently mutated are shown in full atoms (e.g., M182T), the catalytic serine residue (S70) and the N- and C-terminus are indicated. Residues are numbered in agreement with Ambler *(38)*. Most mutated amino acid residues are located near to the protein surface. The figure was drawn using SWISS-PDB Viewer ***(31)***.

in individual optimized variants were always scattered throughout the entire structure and were never clustered adjacent to the site of deletion.

3.7. Construction of Full-Length Mutants

Optimized clone NΔ5-S3/6 was re-elongated to elucidate to what extent the set of mutations compensating for protein destabilization after terminal truncation affect the complete enzyme. The full-length clone named FL-S3/6 was constructed by adding the missing residues according to the schematic representation shown in **Fig. 2A**. This variant was designed for translocation to the periplasm and was expressed in *Escherichia coli* XL-1 Blue cells to probe its functionality in vivo. Unexpectedly, the numbers of colonies on plates (20 h at 37°C) containing chloramphenicol and 100 µg/mL ampicillin was only 50% of the number of

colonies grown on control plates without ampicillin. This was in contrast to NΔ5-S3/6, which grew equally well on both plates. To distinguish between protein function and protein translocation, enzymatic activities of crude whole-cell extracts of FL-S3/6 were tested relative to the nonextended mutant, NΔ5-S3/6. No significant differences in hydrolase activity with the chromogenic substrate nitrocefin were observed, hinting that enzyme translocation could be the main reason. In agreement with these data, decreased cleavage of the signal sequence of clone FL-S3/6 was also observed in the purification process (*see* **Subheading 3.8.**). Consequently, a cytosolically expressed variant was cloned (FL-S3/6-cyt) by replacing the signal sequence and the Asp–Gly tag by a methionine start codon. To ensure correct biophysical comparisons, the analogous construct for wt lactamase (wt-clone-cyt) was cloned.

3.8. Protein Expression and Purification

The generated β-lactamase variants (wt-clone periplasmatic, wt-clone-cyt, NΔ5-clone, optimized mutants NΔ5-S3/6 and NΔ5-S3/7, and FL-S3/6-cyt) were expressed with a His_5-tag in *E. coli* under control of the lac promoter (**Subheading 3.8.1.**). Primarily, two purification steps were applied, first, a substrate analog affinity chromatography using phenylboronate (**Subheading 3.8.2.**), and, second, an IMAC (**Subheading 3.8.3.**). This purification procedure worked very well for the deletion mutant, NΔ5-clone (**Fig. 5**), and the optimized deletion mutant, NΔ5-S3/7.

With some variants of β-lactamase (wt-clone, optimized deletion mutant NΔ5/S3-6, and re-elongated mutant FL-S3/6), purified native enzymes were highly contaminated (30–65%; *see* **Note 7**) with their respective unprocessed forms, most likely because of overexpression and/or rapid folding. Because even a periplasmic extraction aiming at a high product yield resulted in contaminants, a hydrophobic interaction chromatography (HIC) was chosen to separate the native from the much more hydrophobic unprocessed form (**Subheading 3.8.4.**).

Cytoplasmatically expressed β-lactamase variants wt-clone-cyt and FL-S3/6-cyt were purified by phenylboronate affinity chromatography and IMAC. To further increase purity for biophysical characterization, an additional anion exchange chromatography was carried out (**Subheading 3.8.5.**).

3.8.1. Protein Expression and Cell Disruption

1. Transform the vector in cells suitable for protein expression (e.g., BL21).
2. Inoculate 2YT/Cm overnight cultures from glycerol stocks and grow at 28°C for approx 16 to 18 h (*see* **Note 8**).
3. For the expression culture, inoculate four 1-L 2YT/Cm with the overnight culture to obtain a starting OD_{600} of 0.15, and grow at 24°C for the NΔ5 clone, and at 25 to 30°C for all other constructs (*see* **Note 9**).

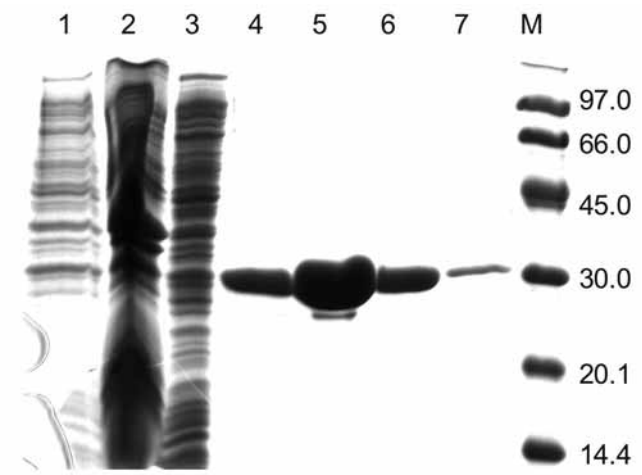

Fig. 5. Expression and purification of the initial β-lactamase deletion mutant (NΔ5-clone). A 12.5% SDS-PAGE, Coomassie stained, shows samples collected before and after purification by phenylboronate (PheBo) and IMAC, respectively. Lane 1, whole-cell lysate before induction; lane 2, whole cell lysate after induction; lane 3, disrupted cell supernatant; lanes 4–7, IMAC elution peak fractions; M, molecular weight marker with individual molecular weights (kDa) indicated.

4. Induce protein expression at OD_{600} of 0.7 with 0.5 m*M* IPTG. Forty minutes after induction, add 100 μg/mL ampicillin to select for β-lactamase-producing cells.
5. Harvest cells after 4 to 5 h (OD_{600} is ~4–5) at 6000*g* in a GS-3 rotor, and freeze the pellet at –80°C.
6. For purification, resuspend one pellet (from 1-L expression culture) in resuspension buffer (*see* **Note 10**) with 200 U benzonase.
7. Disrupt cells in a French press at approx 97 MPa (~14,000 psi) with 5 to 6 cycles in a prechilled cell. Hold samples on ice whenever possible.
8. Clarify crude cell extracts by centrifugation for 40 min at 41,000*g* in a SS-34 rotor at 4°C. Filtrate supernatant using 0.45-μm polyethersulfone syringe filters.

3.8.2. Phenylboronate Affinity Chromatography

1. Equilibrate a 2-mL phenylboronate column with resuspension buffer, load samples from **Subheading 3.8.1., step 8** and wash with resuspension buffer until absorbance at 280 nm approaches baseline.
2. Elute β-lactamase variants with borate buffer.
3. Assess purity by 12.5% sodium dodecyl sulfate (SDS)-polyacrylamide gel electrophoresis (PAGE) followed by Coomassie staining.

3.8.3. Immobilized Metal Ion Affinity Chromatography

1. Equilibrate a 4-mL Ni-NTA column with phosphate buffer with or without 5 m*M* imidazole, and load the samples from **Subheading 3.8.2., step 2**.

2. Wash and elute samples using a step gradient (5, 10, 16, and 100%) of imidazole buffer.
3. Assess purity by 12.5% SDS-PAGE followed by Coomassie staining.
4. For further characterization, dialyze (~8 h) protein samples against three times 1 L of phosphate buffer containing an additional 1 m*M* EDTA in the first dialysis.

3.8.4. Hydrophobic Interaction Chromatography

1. Equilibrate a 1-mL phenylsuperose column with 1 *M* $(NH_4)SO_4$.
2. Supplement the sample from **Subheading 3.8.3., step 2** or from **Subheading 3.8.2., step 2** with ammonium sulfate crystals to a final concentration of 1 *M* $(NH_4)SO_4$ (*see* **Note 11**), and clear the sample by centrifugation (10 min at 27,000*g* and 4°C; SS-34 rotor) and filtration (0.45-µm syringe filter).
3. Load sample onto the HIC column and apply a linear gradient (30 mL) from 0 to 100% of 0.5X phosphate buffer. Because the more hydrophobic unprocessed form should bind more tightly to the column than the processed form, both forms should elute as separate peaks.
4. If HIC chromatography is applied directly after phenylboronate affinity chromatography, the sample is subsequently purified via IMAC, as described in **Subheading 3.8.3**.

3.8.5. Anion Exchange Chromatography

1. Dialyze samples from **Subheading 3.8.3., step 2** three to four times in 1 to 1.5 L of Tris-HCI buffer.
2. Equilibrate a Mono Q anion exchange column with Tris-HCI buffer and load the sample.
3. Elute with a 30 mL linear gradient from 0 to 100% of Tris-HCI–NaCl buffer.
4. Dialyze the eluted protein as described in **Subheading 3.8.3., step 4**.

Amino acid compositions of all variants were confirmed by electrospray mass spectrometry within typical deviations from calculated masses. Enzymes were dialyzed as described in **Subheading 3.8.3., step 4** and characterized within 1 wk after purification. Before use, enzyme solutions were clarified by centrifugation (30 min at 15000*g* and 10°C). Protein concentrations were taken from absorbance spectra at 280 nm (*see* **Note 12**).

3.9. Enzyme Assays

The kinetic parameters of the β-lactamase variants were assayed photospectrometrically at 486 nm, using the chromogenic substrate nitrocefin ($\Delta\varepsilon_{486}$ = 16,000/M/cm).

1. Add 20 µL of enzyme dilution to 980 µL nitrocefin solution, mix, and immediately measure the change in absorbance at 486 nm for approx 1 min (*see* **Note 13**). We used a final enzyme concentration of 2.5 n*M* for the initial deletion mutant and 0.5 n*M* for all other variants.
2. Repeat measurements at least twice and calculate standard deviations.

Table 2
Kinetic Parameters

β-Lactamase variant	k_{cat} (1/s)	K_M (μ*M*)	k_{cat}/K_M (/M/s)
Wt-clone	780 ± 9	84.4	9.24×10^6
NΔ5-clone	123 ± 2	61	2.02×10^6
NΔ5-S3/6	728 ± 7	58.9	12.4×10^6
NΔ5-S3/7	732 ± 19	64.3	11.4×10^6
Wt-clone-cyt	602 ± 8	52.2	11.5×10^6
FL-S3/6-cyt	633 ± 9	70.6	8.97×10^6

Kinetic constants were determined at 25°C in 50 m*M* potassium phosphate buffer, 0.5% dimethylsulfoxide, pH 7.0, using the β-lactam compound nitrocefin as substrate.

3.9.1. Determination of Michaelis Constant and Turnover Number

1. To determine Michaelis constant (K_M) values, measure initial rates with substrate concentrations ranging from 10 to 500 μ*M* and enzyme concentrations of 2.7 to 5.9 n*M* for the NΔ5-clone and 0.5 n*M* for all other mutants.
2. Fit data to the Michaelis-Menten equation using, e.g., the Marquardt-Levenberg algorithm implemented in the program SigmaPlot (SPSS).

The K_M of NΔ5-clone approximated that of wt-clone, but the turnover number (k_{cat}) decreased approximately sixfold, implying an active site organization sufficient for binding but not for effective catalysis (**Table 2**).

3.9.2. Thermoactivity Profiles and Half-Life Time

To test and compare the temperature dependency of activity and the kinetics of heat-induced inactivation, a thermoactivity screen can be used. We assayed turnover rates at increasing temperatures (25–70°C) after specific incubation times (**Fig. 6**).

1. To assess thermoactivity, prepare a 292 n*M* solution for NΔ5-clone and a 25 n*M* solution for all other variants, and split these into three aliquots.
2. Incubate the first aliquot for 5 min at a given temperature (25–70°C) in a heated water bath and keep both of the remaining samples on ice.
3. Before measurement, mix the respective sample by brief vortexing.
4. Transfer 20 μL of the sample to 980 μL of nitrocefin solution preheated to the respective assay temperature, and determine the initial reaction rate between 5 and 25 s in a heated spectrophotometer.
5. Preheat the second aliquot for 30 s at the respective temperature, and assay as detailed in **steps 3** and **4**.
6. Assay the third aliquot after 10 min incubation on ice.
7. Repeat the entire procedure for a different temperature.

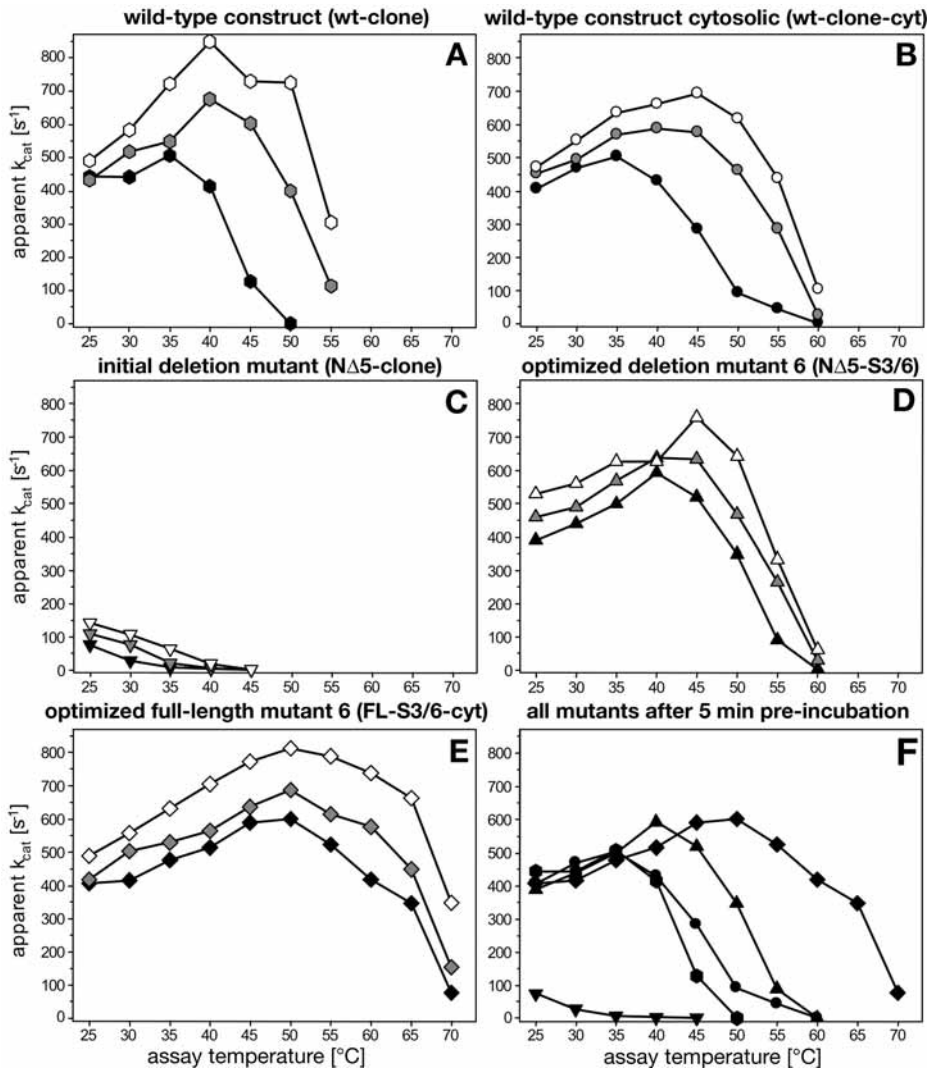

Fig. 6. Temperature-dependent activity profiles of investigated β-lactamase variants. **(A–E)** apparent k_{cat} values were determined photospectrometrically from 25 to 70°C, using nitrocefin as the substrate. Enzyme solutions are diluted (initial deletion mutant: 292 n*M*, all other mutants: 25 n*M*), split into three fractions, and subjected to different pretreatments: incubation for 5 min or 30 s at assay temperature (black and grey symbols, respectively), or storage on ice for 10 min (white symbols). Assay buffer (980 µL) was prewarmed in a heated water bath before the reactions were started by adding 20 µL of enzyme solution. Final enzyme concentrations of 5.9 n*M* for the initial deletion mutant and 0.5 n*M* for all other variants were used. **(F)** Summary of thermoactivity profiles obtained after 5-min preincubation. ⬢, wt-clone (periplasmatic); ●, wt-clone (cytosolic); ▼, NΔ5-clone; ▲, NΔ5-S3/6; ◆, FL-S3/6-cyt.

The thermoactivity profiles of the wt-clone varied clearly depending on the pretreatment (**Fig. 6A**). The temperature optimum after ice incubation and 30 s preheating at the assay temperature was 40°C. However, when the enzyme was preheated for 5 min, the maximum shifted down to 35°C, indicating commencing thermal unfolding.

The truncated NΔ5-clone maintained its highest activity at 25°C, the lowest temperature examined (**Fig. 6C**). With increasing temperatures, enzyme activity dropped rapidly and approached zero at 40°C. A detailed analysis of the reaction rate at 40°C after incubation on ice showed that this mutant was heat inactivated during the measurement, within seconds after addition to the preheated assay mixture (**Fig. 7A**). The observed decrease of reaction rate over time could be fitted by an exponential decay equation (*see* **Note 14**), yielding a half-life time of 7 s at 40°C (**Fig. 7B**).

The 0- and 30-s temperature–activity profiles of the optimized mutant NΔ5-S3/6 (**Fig. 6D**) largely resembled those of the wt-clone. However, the 5-min preheating profile differed significantly. The temperature–activity curve of this optimized mutant was shifted to higher temperatures by approx 8°C compared with the wt-clone (**Fig. 6A**,**F**).

The full-length optimized mutant, FL-S3/6-cyt (**Fig. 6E**), exhibited thermostability features superior to those of the optimized deletion mutant, NΔ5-S3/6, and the corresponding wt-clone-cyt (**Fig. 6B**,**F**). The catalytic activities of these clones were nearly identical at assay temperatures up to 40°C, irrespective of pretreatment. At 50°C and greater, FL-S3/6-cyt retained significant higher activities, especially at conditions of prolonged heat stress of 5-min preincubation. The maximum catalytic activity of wt-clone-cyt was at 45°C after ice incubation, but decreased to 35°C after 5 min of preincubation. In contrast, the temperature optimum of FL-S3/6-cyt (50°C) remained unchanged. Only the reaction rate decreased after heat incubation. Interestingly, the alterations between wt-clone and wt-clone-cyt at the N terminus (AspGly replaced by Met) influenced stability.

Comparison of the 5-min preincubation thermoactivity profiles of all truncated and full-length variants (**Fig. 6F**) illustrates how terminal truncation diminished activity at 35 to 40°C. Compensating amino acid substitutions restored activity and even improved stability. Re-extension of optimized mutant S3/6 further increased thermostability as well as thermoactivity.

3.10. Urea-Induced Unfolding and Data Analysis

Unfolding of the β-lactamase variants was evaluated by fluorescence spectroscopy. The red-shift of the intrinsic tryptophan fluorescence emission maximum was monitored as a function of urea concentration (**Fig. 8**, **Table 3**). Data analysis was performed according to a three-state model.

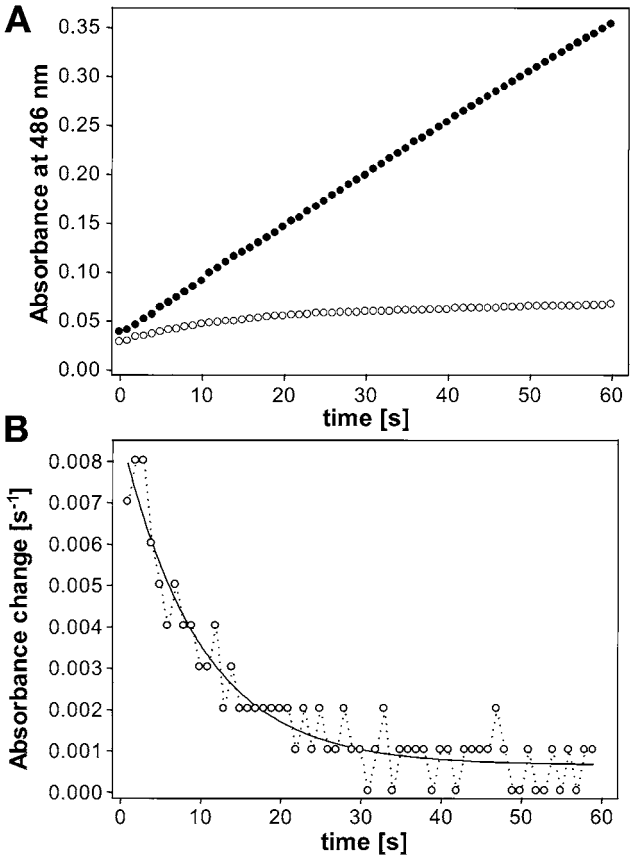

Fig. 7. Enzyme kinetics and exponential decay of catalytic activity of NΔ5-clone and stable kinetics of NΔ5-S3/6 at 40°C. **(A)** Spectrophotometric analysis of product formation using the chromogenic substrate nitrocefin. The final enzyme concentration was 2.9 n*M* for NΔ5-clone (¡) and 0.5 n*M* for NΔ5-S3/6 clone (●). Twenty microliters of a concentrated enzyme solution was mixed with 980 µL of prewarmed assay buffer. **(B)** Exponential decay fit of enzymatic activity of NΔ5-clone using the change of absorbance per second (ΔA/Δt) from the data shown in (A). A three-parameter exponential decay fit revealed a half-life of 7 s at 40°C (using *SigmaPlot*).

1. Equilibrate 300 to 400 n*M* enzyme solutions from **Subheading 3.8.3., step 4** containing 0.25 to 8 *M* urea for 18 to 20 h at 19°C.
2. Record fluorescence emission spectra from 320 to 380 nm at 20 to 23°C while exciting at 280 nm. For each data point, average four scans.
3. If necessary, correct fluorescence spectra for the background fluorescence of the solution (phosphate buffer plus denaturant).

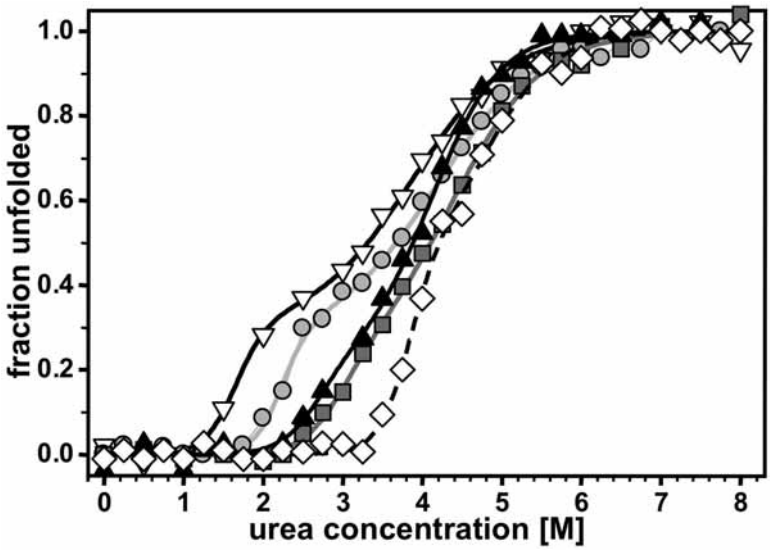

Fig. 8. Unfolding of β-lactamase variants in urea. Denaturation is followed using the red-shift of intrinsic fluorescence emission maxima. Enzyme samples (0.3–0.4 m*M* in 50 m*M* sodium phosphate and 150 m*M* NaCl, pH 7.2) containing 0.25 to 8 *M* urea were equilibrated for 18 to 20 h at 19°C and measured at 20°C to 23°C. Data are fitted assuming a three-state unfolding mechanism. NΔ5-clone, inverted triangles (white); wt-clone-cyt, circles (light grey); optimized deletion mutant NΔ5-S3/7, squares (dark grey); mutant NΔ5-S3/6, triangles (black); and optimized full-length mutant FL-S3/6-cyt, diamonds (white, dashed line).

Table 3
Thermodynamic Parameters

Variant	$\Delta G^0_{NI, H_20}$ (kJ/mol)	m_{NI} (kJ/mol/*M*)	$D^{1/2}_{NI}$ (/*M*)	$\Delta G^0_{IU, H_20}$ (kJ/mol)	m_{IU} (kJ/mol/*M*)	$D^{1/2}_{IU}$ (/*M*)
Wt-clone-cyt	30.4 ± 4.5	13.7 ± 2.1	2.9	15.8 ± 1.1	3.8 ± 0.2	4.2
NΔ5-clone	20.2 ± 5.5	12.3 ± 3.7	1.6	15.3 ± 1.7	3.9 ± 0.4	3.9
NΔ5-S3/7	27.1 ± 6.4	9.3 ± 2.6	2.9	19.0 ± 2.6	4.3 ± 0.5	4.4
NΔ5-S3/6	26.2 ± 10.1	9.8 ± 4.3	2.7	23.4 ± 3.2	5.7 ± 0.6	4.1
FL-S3/6-cyt	45.8 ± 7.7	11.9 ± 2.2	3.8	27.2 ± 7.0	5.6 ± 1.2	4.9

Data were analyzed using the linear extrapolation method ***(49)*** assuming a biphasic unfolding transition (native, intermediate, and unfolded). The values for half denaturation were obtained according to **Eq. 2** (**Subheading 3.10., step 7**).

4. Smooth the fluorescence intensity spectra to obtain the associated λ_{max} values. We used a tricube weighting function (Loess; sampling proportion, 0.25; polynomial degree, 3) implemented in the program Sigma Plot (**Note 15**).
5. Analyze the data assuming an appropriate model for the unfolding reaction.

6. For a three-state model, N ⇌ I ⇌ U (where N resembles the native, I the intermediate, and U the unfolded state), with two equilibrium constants, K_{NI} and K_{IU}, fit the thermodynamic parameters $\Delta G^0_{NI,H_2O}$, $\Delta G^0_{IU,H_2O}$, m_{NI}, m_{IU}, and y_I to the fluorescent data using the following equation (*see* **Note 16**):

$$y_{obs} = \frac{y_N + y_I \times e^{\left(\frac{-\Delta G^0_{NI,H_2O} + m_{NI} \times [D]}{R \times T}\right)} + y_U \times e^{\left(\frac{-\Delta G^0_{NI,H_2O} + m_{NI} \times [D]}{R \times T}\right)} \times e^{\left(\frac{-\Delta G^0_{IU,H_2O} + m_{IU} \times [D]}{R \times T}\right)}}{1 + e^{\left(\frac{-\Delta G^0_{NI,H_2O} + m_{NI} \times [D]}{R \times T}\right)} + e^{\left(\frac{-\Delta G^0_{NI,H_2O} + m_{NI} \times [D]}{R \times T}\right)} \times e^{\left(\frac{-\Delta G^0_{IU,H_2O} + m_{IU} \times [D]}{R \times T}\right)}} \quad (1)$$

   Set y_N and y_U to the average of the first and last data points, respectively. A slope in the baselines was not seen in our case.
7. The midpoints of transitions are given by:

$$[D]_{1/2} = \frac{\Delta G^O_{H_2O}}{m} \quad (2)$$

The order of denaturation (**Fig. 8**, *see* **Note 17**) corresponded to the order seen in the thermoactivity assays (**Fig. 6** and **Subheading 3.9.2.**). The NΔ5-clone was the least stable, followed by the wt-clone-cyt. The optimized mutants, NΔ5-S3/6 and NΔ5-S3/7, started to unfold at approximately the same urea concentration, and the elongated FL-S3/6 was the last one to unfold.

The unfolding showed a clear three-state behavior in the case of the wt-clone-cyt and the NΔ5-clone. Taking a closer look at the FL/S3-6-cyt data and comparing two- and three-state fits also strongly indicated a three-state behavior. The data of the optimized mutants, NΔ5-S3/6 and NΔ5-S3/7, could be explained either by a two- or three-state unfolding. For comparison, all data were fitted using the three-state model, N ⇌ I ⇌ U with **Eq. 1** (*see* **step 6** and **Table 3**). This approach is supported by previously described intermediate folding states for TEM-type β-lactamases ***(42–44)***. Enzyme activity tests with urea-denatured proteins showed decreasing activity after first denaturation. The extracted thermodynamic values aid in the comparison and explanation of the obtained mutants, but require careful interpretation because of underlying assumptions. The deletion of five N-terminal amino acids primarily affected the first transition, reducing the stability by approx 10 kJ/mol and had little effect on the second transition. Optimizing for catalytic activity in vivo yielded clones displaying stabilization effects for both transitions, whereby the achieved stability of the first transition is below and the second is above the wt-clone. Elongation (clone FL-3/6-cyt) considerably stabilized the first phase (19.6 kJ/mol compared with NΔ5-S3/6), but had little effect on the second transition (3.8 kJ/mol compared with NΔ5-S3/6). This is in agreement with the view that elongation compensated truncation independent of the introduced mutations. Comparing FL-S3/6-cyt with wt-clone-cyt revealed a stabilization of 15 kJ/mol

for the first transition, and of 11.4 kJ/mol for the second transition. It is important to note that the optimized mutants denature at higher urea concentrations than the wt-clone, confirming the stability ranking observed in the thermoactivity assays.

4. Notes

1. To ensure that growth results can be compared, a preculture is required to provide consistent starting conditions.
2. The error rate of the shuffling process was determined to be 0.83 by analysis of 2529 bases.
3. Elution of bound the DNA fragment is increased by elongated incubation (15 min) at elevated temperatures, e.g., 50°C.
4. No extra primers are added at this point to facilitate mutual priming and shuffling of the isolated DNA fragments.
5. Increased Mg^{2+} concentrations stabilize noncomplementary basepairs, whereas the presence of 0.5 m*M* manganese ions diminishes the template specificity of the polymerase. Error rates can be controlled over a wide range, for example, by varying the number of template molecules, the cycle number, the period of extension, the source and amount of polymerase, the concentrations and ratios of dNTPs, and the type of dNTP analogs used. The error rate also depends on the nucleotide composition of the target gene. Thus, the use of an identical protocol may give quite different results in different trials.
6. If the enzyme activity is very low in the first round, selection can alternatively be performed in liquid medium (LB/Cm with different amounts of ampicillin), where the selection stringency is lower than on plates.
7. The percent of unprocessed protein was quantified from scanned Coomassie-stained gels using the image analysis software, Scion/NIH image.
8. If expression is performed at temperatures significantly below 37°C, it is best to also lower the temperature of the overnight culture to avoid a lag phase when starting the expression culture.
9. The optimal expression temperature needs to be adjusted for every mutant by performing a small-scale growth test at various temperatures.
10. Two pH values (7.0 and 7.2) were tested, with equal results.
11. 1 *M* $(NH_4)SO_4$ is desirable to ensure proper binding, but, if protein precipitation is a problem, the concentration of $(NH_4)SO_4$ can be reduced. Because samples with wt β-lactamase started to precipitate after addition of 0.5 *M* $(NH_4)SO_4$, a final concentration of only 0.65 *M* was used. In this case, the native form of the enzyme was in the flow-through, whereas the unprocessed form was retained on the column.
12. Absorbance spectra were measured from 350 to 220 nm, and the absorption at 280 nm was corrected for background absorbance by extrapolating the absorbance between 320 and 350 nm linearly to 280 nm. Molar extinction coefficients and molecular masses were calculated according to Gill and Hippel ***(45)***.

13. Because the first seconds of the reaction are especially important for enzymes with very short half-lifes, it is essential to start the measurement immediately after adding the enzyme. In addition, instruments should be used that record at least one data point per second.
14. The enzyme decay was fitted using the three-parameter exponential decay fit implemented in SigmaPlot: $\frac{\Delta A}{\Delta t} = a + \left[\frac{\Delta A}{\Delta t}\right]_0 e^{-\lambda \times t}$ whereby a is a parameter accounting for basal and accumulated absorption of the nitrocefin solution and $T_{1/2} = \ln 2/\lambda$
15. Depending on the number of data points per nanometer acquired, the parameters for smoothing need to be adjusted. Alternatively, a running mean average can be used for smoothing. In addition to determining λ_{max}, we also tested the shift of center of mass from 330 to 370 nm. Despite the use of more data points, this method did not necessarily give better results.
16. The emission maximum (y_{obs}) as a function of denaturant concentration, [D], was deconvoluted in the constituting signals of the three conformational states (y_N, y_I, y_U) according to their fraction present (f_N, f_I, f_U), which is described by $y_{obs} = y_N \times f_N + y_I \times f_I + y_U \times f_U$. The law of mass action, $K_{NI} = [I]/[N]$, $K_{IU} = [U]/[I]$, was combined with mass conservation, $[N]_0 = [N] + [I] + [U]$, to calculate the fractions, $f_N = 1/(1 + K_{NI} + K_{NI} \times K_{IU})$, $f_I = K_{NI}/(1 + K_{NI} + K_{NI} \times K_{IU})$, and $f_U = K_{NI} \times K_{IU}/(1 + K_{NI} + K_{NI} \times K_{IU})$. Thermodynamic parameters were introduced using the linear extrapolation method based on $\Delta G^0 = -RT\ln K = \Delta G^0_{H_2O} - m \times [D]$, assuming a linear dependence for all states ***(46)***.
17. To account for small changes between the absolute maxima measured with the two fluorometers, the normalized fraction unfolded, $f_{unfold} = (y_{obs} - y_F)/(y_U - y_F)$, is given in the plot.

References

1. Jaenicke, R. and Böhm, G. (1998) The stability of proteins in extreme environments. *Curr. Opin. Struct. Biol.* **8,** 738–748.
2. Ladenstein, R. and Antranikian, G. (1998) Proteins from hyperthermophiles: stability and enzymatic catalysis close to the boiling point of water. *Adv. Biochem. Eng. Biotechnol.* **61,** 37–85.
3. Querol, E., Perez-Pons, J. A., and Mozo-Villarias, A. (1996) Analysis of protein conformational characteristics related to thermostability. *Protein Eng.* **9,** 265–271.
4. Vieille, C. and Zeikus, G. J. (2001) Hyperthermophilic enzymes: sources, uses, and molecular mechanisms for thermostability. *Microbiol. Mol. Biol. Rev.* **65,** 1–43.
5. Pace, C. N., Grimsley, G. R., Thomson, J. A., and Barnett, B. J. (1988) Conformational stability and activity of ribonuclease T1 with zero, one, and two intact disulfide bonds. *J. Biol. Chem.* **263,** 11,820–11,825.
6. Mason, J. M., Gibbs, N., Sessions, R. B., and Clarke, A. R. (2002) The influence of intramolecular bridges on the dynamics of a protein folding reaction. *Biochemistry* **41,** 12,093–12,099.

7. Thompson, M. J. and Eisenberg, D. (1999) Transproteomic evidence of a loop-deletion mechanism for enhancing protein thermostability. *J. Mol. Biol.* **290,** 595–604.
8. Vogt, G., Woell, S., and Argos, P. (1997) Protein thermal stability, hydrogen bonds, and ion pairs. *J. Mol. Biol.* **269,** 631–643.
9. Szilagyi, A. and Zavodszky, P. (2000) Structural differences between mesophilic, moderately thermophilic and extremely thermophilic protein subunits: results of a comprehensive survey. *Structure Fold Des* **8,** 493–504.
10. Karshikoff, A. and Ladenstein, R. (2001) Ion pairs and the thermotolerance of proteins from hyperthermophiles: a "traffic rule" for hot roads. *Trends Biochem. Sci.* **26,** 550–556.
11. Petsko, G. A. (2001) Structural basis of thermostability in hyperthermophilic proteins, or "there's more than one way to skin a cat." *Methods Enzymol.* **334,** 469–478.
12. Malakauskas, S. M. and Mayo, S. L. (1998) Design, structure and stability of a hyperthermophilic protein variant. *Nat. Struct. Biol.* **5,** 470–475.
13. Filikov, A. V., Hayes, R. J., Luo, P., et al. (2002) Computational stabilization of human growth hormone. *Protein Sci.* **11,** 1452–1461.
14. Lehmann, M., Loch, C., Middendorf, A., et al. (2002) The consensus concept for thermostability engineering of proteins: further proof of concept. *Protein Eng.* **15,** 403–411.
15. Stemmer, W. P. (1994) Rapid evolution of a protein in vitro by DNA shuffling. *Nature* **370,** 389–391.
16. Stemmer, W. P. (1994) DNA shuffling by random fragmentation and reassembly: in vitro recombination for molecular evolution. *Proc. Natl. Acad. Sci. USA* **91,** 10,747–10,751.
17. Yang, F., Cheng, Y., Peng, J., Zhou, J., and Jing, G. (2001) Probing the conformational state of a truncated staphylococcal nuclease R using time of flight mass spectrometry with limited proteolysis. *Eur. J. Biochem.* **268,** 4227–4232.
18. Van der Schueren, J., Robben, J., and Volckaert, G. (1998) Misfolding of chloramphenicol acetyltransferase due to carboxy-terminal truncation can be corrected by second-site mutations. *Protein Eng.* **11,** 1211–1217.
19. Sherwood, L. M. and Potts, J. T., Jr. (1965) Conformational studies of pancreatic ribonuclease and its subtilisin-produced derivatives. *J. Biol. Chem.* **240,** 3799–3805.
20. Haruki, M., Noguchi, E., Akasako, A., Oobatake, M., Itaya, M., and Kanaya, S. (1994) A novel strategy for stabilization of Escherichia coli ribonuclease HI involving a screen for an intragenic suppressor of carboxyl-terminal deletions. *J. Biol. Chem.* **269,** 26,904–26,911.
21. Trevino, R. J., Tsalkova, T., Kramer, G., Hardesty, B., Chirgwin, J. M., and Horowitz, P. M. (1998) Truncations at the NH2 terminus of rhodanese destabilize the enzyme and decrease its heterologous expression. *J. Biol. Chem.* **273,** 27,841–27,847.
22. Trevino, R. J., Gliubich, F., Berni, R., et al. (1999) NH2-terminal sequence truncation decreases the stability of bovine rhodanese, minimally perturbs its crystal structure, and enhances interaction with GroEL under native conditions. *J. Biol. Chem.* **274,** 13,938–13,947.

23. Vainshtein, I., Atrazhev, A., Eom, S. H., Elliott, J. F., Wishart, D. S., and Malcolm, B. A. (1996) Peptide rescue of an N-terminal truncation of the Stoffel fragment of taq DNA polymerase. *Protein Sci.* **5,** 1785–1792.
24. Shortle, D. and Lin, B. (1985) Genetic analysis of staphylococcal nuclease: identification of three intragenic "global" suppressors of nuclease-minus mutations. *Genetics* **110,** 539–555.
25. Petrounia, I. P. and Arnold, F. H. (2000) Designed evolution of enzymatic properties. *Curr. Opin. Biotechnol.* **11,** 325–330.
26. Krebber, A., Bornhauser, S., Burmester, J., et al. (1997) Reliable cloning of functional antibody variable domains from hybridomas and spleen cell repertoires employing a reengineered phage display system. *J. Immunol. Methods* **201,** 35–55.
27. Orencia, M. C., Yoon, J. S., Ness, J. E., Stemmer, W. P., and Stevens, R. C. (2001) Predicting the emergence of antibiotic resistance by directed evolution and structural analysis. *Nat. Struct. Biol.* **8,** 238–242.
28. Rodrigues, M. L., Presta, L. G., Kotts, C. E., et al. (1995) Development of a humanized disulfide-stabilized anti-p185HER2 Fv-beta-lactamase fusion protein for activation of a cephalosporin doxorubicin prodrug. *Cancer Res.* **55,** 63–70.
29. Huang, W. and Palzkill, T. (1997) A natural polymorphism in beta-lactamase is a global suppressor. *Proc. Natl. Acad. Sci. USA* **94,** 8801–8806.
30. Shindyalov, I. N. and Bourne, P. E. (1998) Protein structure alignment by incremental combinatorial extension (CE) of the optimal path. *Protein Eng.* **11,** 739–747.
31. Guex, N. and Peitsch, M. C. (1997) SWISS-MODEL and the Swiss-PdbViewer: an environment for comparative protein modeling. *Electrophoresis* **18,** 2714–2723.
32. Huang, W., Petrosino, J., Hirsch, M., Shenkin, P. S., and Palzkill, T. (1996) Amino acid sequence determinants of beta-lactamase structure and activity. *J. Mol. Biol.* **258,** 688–703.
33. Lei, S. P., Lin, H. C., Wang, S. S., Callaway, J., and Wilcox, G. (1987) Characterization of the Erwinia carotovora pelB gene and its product pectate lyase. *J. Bacteriol.* **169,** 4379–4383.
34. Yanisch-Perron, C., Vieira, J., and Messing, J. (1985) Improved M13 phage cloning vectors and host strains: nucleotide sequences of the M13mp18 and pUC19 vectors. *Gene* **33,** 103–119.
35. Olins, P. O., Devine, C. S., Rangwala, S. H., and Kavka, K. S. (1988) The T7 phage gene 10 leader RNA, a ribosome-binding site that dramatically enhances the expression of foreign genes in Escherichia coli. *Gene* **73,** 227–235.
36. Cadwell, R. C. and Joyce, G. F. (1994) Mutagenic PCR. *PCR Methods Appl.* **3,** S136–S140.
37. Jelsch, C., Mourey, L., Masson, J. M., and Samama, J. P. (1993) Crystal structure of Escherichia coli TEM1 beta-lactamase at 1.8 A resolution. *Proteins* **16,** 364–383.
38. Ambler, R. P., Coulson, A. F., Frere, J. M., et al. (1991) A standard numbering scheme for the class A beta-lactamases. *Biochem. J.* **276 (Pt 1),** 269, 270.
39. Sideraki, V., Huang, W., Palzkill, T., and Gilbert, H. F. (2001) A secondary drug resistance mutation of TEM-1 beta-lactamase that suppresses misfolding and aggregation. *Proc. Natl. Acad. Sci. USA* **98,** 283–288.

40. Wang, X., Minasov, G., and Shoichet, B. K. (2002) Evolution of an antibiotic resistance enzyme constrained by stability and activity trade-offs. *J. Mol. Biol.* **320,** 85–95.
41. Osuna, J., Perez-Blancas, A., and Soberon, X. (2002) Improving a circularly permuted TEM-1 beta-lactamase by directed evolution. *Protein Eng.* **15,** 463–470.
42. Vanhove, M., Raquet, X., and Frere, J. M. (1995) Investigation of the folding pathway of the TEM-1 beta-lactamase. *Proteins* **22,** 110–118.
43. Zahn, R., Axmann, S. E., Rucknagel, K. P., Jaeger, E., Laminet, A. A., and Plückthun, A. (1994) Thermodynamic partitioning model for hydrophobic binding of polypeptides by GroEL. I. GroEL recognizes the signal sequences of beta-lactamase precursor. *J. Mol. Biol.* **242,** 150–164.
44. Frech, C., Wunderlich, M., Glockshuber, R., and Schmid, F. X. (1996) Competition between DsbA-mediated oxidation and conformational folding of RTEM1 beta-lactamase. *Biochemistry* **35,** 11,386–11,395.
45. Gill, S. and von Hippel, G. (1989) Calculation of protein extinction coefficients from amino acid sequence data. *Anal. Biochem.* **182,** 319–326.
46. Pace, C. N. (1986) Determination and analysis of urea and guanidine hydrochloride denaturation curves. *Methods Enzymol.* **131,** 266–280.
47. Sayle, R. A. and Milner-White, E. J. (1995) RASMOL: biomolecular graphics for all. *Trends Biochem. Sci.* **20,** 374.
48. Vriend, G. (1990) WHAT IF: a molecular modeling and drug design program. *J. Mol. Graph.* **8,** 52–56.
49. Santoro, M. M. and Bolen, D. W. (1988) Unfolding free energy changes determined by the linear extrapolation method. 1. Unfolding of phenylmethanesulfonyl alpha-chymotrypsin using different denaturants. *Biochemistry* **27,** 8063–8068.